Supplementary information to ”Storm swells across the Pacific”

Fabrice Ardhuin[1*], Bertrand Chapron[2], and Fabrice Collard[3],

[1]Service Hydrographique et Ocanographique de la Marine, 29609 Brest, France
[2]Laboratoire d’Océanographie Spatiale, Ifremer,
Centre de Brest, 29280 Plouzané, France
[3]BOOST-Technologies, 29280 Plouzané, France

[*]To whom correspondence should be addressed; E-mail: ardhuin@shom.fr.

1 SAR products and database generation

All SAR products used here are level 2 products that provided by ESA and processed or re-processed to the standard of the operational products as of November 2007. We note that real-time level 2 products generated before November 2007 have systematic errors and were frequently of poor quality due to artefacts caused by a faulty filtering of the radar images. This filtering is necessary to remove patterns that are not related to the sea state (slicks, ships ...). The products used here contain the directional wave spectrum without directional ambiguity and additional data that include the backscatter-derived wind speed for which a model wind direction is used, provided by analyses from the European Center for Medium Range Weather Forecasting (ECMWF). That information will be used in our analysis. Other information on the image normalized variance, which can be used to flag images with land, ships, slicks or other cuases of backscatter variations not related to the wave field, and the SAR azimuthal cut-off, which can be used to check that swell partitions are fully seen by the SAR, are also provided.

ENVISAT wave mode images are acquired every 100 km looking down to the right of the flight direction, 23° to the right from nadir. The repeat orbit of ENVISAT is 35 days.

1.1 Virtual SAR buoys

A first type SAR wave mode data analysis was performed to verify the capability of SAR to track swell systems. A region of the ocean covering 2 by 2 degrees in latitude and longitude is selected and all data in that square area is combined. For each waves spectrum swell partitions are extracted using standard procedures, and a time history of these partitions is formed. In order to increase the quantity of data, swell partitions from a wider region are propagated in space and time following the theoretical great circle route in the wave direction, at the group speed corresponding to the peak wavelength. In figure 1a, each horizontal colored segment thus corresponds to one swell partition that crosses the spatial window. The segment length corresponds to the time during which the propagated swell system is present in the spatial window. Some segments are very short, corresponding to trajectories that barely cut one corner of the square.

Clearly the SAR detects the directions of the most energetic part of the wave spectrum which is also measured by the buoys.

2 Analysis of SWAO tracks and attenuation estimation

A database of energetic storms was compiled from QuikSCAT and ECMWF analysis wind fields and surface pressure analyses. The full SAR wave mode data was then searched by tracking back swells from each SAR image and each swell partition. A list of 13 storms with long swell generation was then established. From these storm centers detected every 6 hours, great circle tracks were traced in all directions, and tracks away from islands were chosen, using the University of Hawaii global shoreline database to provide information on island positions

(*1*). Each track was followed at a fixed group speed (discrete speeds corresponding to 13, 14, 15, 16, 17, 18 and 19 s wave periods). Along each track, thus defined by its origin in space and time, its outgoing direction θ and the wave period T, all ENVISAT wave mode and ERS-2 and ENVISAT altimeter wave products were gathered with a acceptable time window of plus or minus 3 hours from the theoretical position. For wave mode data, only swell partitions with peak wavelength and direction within 50 m and 20 degrees of expected were retained. Each track thus produced a short ASCII file containing these time and position information, plus the local swell partition height, wavelength and direction, and the local SAR-derived wind speed. These files are available via anonymous ftp at the address `ftp.ifremer.fr` under the directory, `ifremer/cersat/products/gridded/wavewatch3/HINDCAST/SWAO/`

2.1 Swell track combination and SAR data selection

A typical track file contains 3 to 20 SAR data. In order to be able to define stable attenuation of the swell energy, tracks with neighboring values of the outgoing directions are merged, with relatively narrow direction bands, of the order of 5 to 10° (table 1), so that the combined wave properties are similar enough.

A set of 19 of such track ensembles was then selected (table 1), with enough SAR data at large distance from the storm to allow for a reliable estimation of the swell attenuation. These amount to 92 tracks out of the 815 of the original database.

2.2 Verification of geometrical optics asymptotes and point source hypothesis

The asymptotic energy-conserving solution $\propto 1/\left[\phi \sin(\phi)\right]$ was verified using a semi-analytic model. This model uses the conservation of the spectral density along geodesics, which are computed analytically on the spherical Earth. At time $t = 0$ the initial wave spectrum is prescribed to be Gaussian in space and centered on the equator, with a width σ_x. The initial wave

Storm time	T	$\theta_{\min}$	$\theta_{\max}$	N	α (m^{-1})	H_1 (m)	ε	γ (m^{-2})	H_2 (m)
20040216 00	15	85	95	30	21.3×10^{-8}	4.4	17 %	44.1×10^{-8}	5.2
20040327 06	15	37	43	23	6.1×10^{-8}	2.0	11 %	15.9×10^{-8}	2.0
20040418 18	14	63	94	11	21.3×10^{-8}	3.7	15 %	48.6×10^{-8}	4.2
20040418 18	15	85	90	15	8.0×10^{-8}	2.7	9 %	15.9×10^{-8}	2.7
20040418 18	16	69	87	40	8.7×10^{-8}	3.0	10 %	20.9×10^{-8}	3.1
20040418 18	17	75	85	32	4.3×10^{-8}	2.9	10 %	7.6×10^{-8}	2.9
20040630 23	13	75	80	25	5.5×10^{-8}	2.0	28 %	15.6×10^{-8}	2.0
20040709 18	14	32	37	12	11.7×10^{-8}	2.4	6 %	33.8×10^{-8}	2.5
20050330 12	13	45	55	14	9.0×10^{-8}	2.0	18 %	21.9×10^{-8}	2.0
20050330 06	14	35	45	19	9.7×10^{-8}	2.0	12 %	24.1×10^{-8}	2.0
20051021 00	15	120	130	23	9.1×10^{-8}	2.9	10 %	23.1×10^{-8}	3.0
20051021 00	17	135	150	26	3.5×10^{-8}	2.6	18 %	14.4×10^{-8}	2.7
20051114 03	13	90	100	21	13.3×10^{-8}	2.3	11 %	38.8×10^{-8}	2.4
20051114 12	15	85	95	45	11.0×10^{-8}	2.6	15 %	38.3×10^{-8}	2.9
20051115 12	17	80	90	35	7.3×10^{-8}	2.6	14 %	16.4×10^{-8}	2.6
20070212 18	15	75	90	49	33.7×10^{-8}	4.8	10 %	75.5×10^{-8}	7.6
20070324 00	18	71.5	73.5	18	11.0×10^{-8}	2.0	12 %	32.8×10^{-8}	2.0
20070812 00	15	330	336	20	6.6×10^{-8}	2.0	19 %	24.9×10^{-8}	2.0
20071030 00	15	74	82	59	15.6×10^{-8}	2.6	14 %	41.3×10^{-8}	2.7

Table 1: Ensembles of swell tracks selected for swell attenuation analysis. Each ensemble is defined by the source storm, the minimum and maximum outgoing directions $\theta_{\min}$ and $\theta_{\max}$. The number of SAR data that was retained for the estimation of the attenuation is N. The fitted wave height at 4000 km from the source and constant linear decay coefficients are H_1 and α, with ε the mismatch of the linear attenuation to the observed wave heights, normalized by the r.m.s. observed height. The geographical positions of the storm centers are 160 E 37 N for February 2004, 145 E 45 S for March 2004, 165 E 52 S for April 2004, 145 E 25 N for June 2004, that storm is also known as Typhoon Ting-Ting, 177 W 55 S for July 2004 (see figure 1), 47 W 50 S for March 2005, 155 W 50 N for October 2005,160 E 40 N for November 2005, 168 E 38 N for February 2007, 165 W 53 S for March 2007, 100 W 47 S for August 2007 , and 155 W 47 S for October 2007 .

spectrum is prescribed to be a JONSWAP-type spectrum with a peak enhancement factor γ_J ,which is related to a spectral width parameter σ_f. Finally, the initial spectra are taken isotropic in directions. That latter aspect is not very realistic but simplifies the calculations since the initial spectral density is only given by the frequency and not the direction.

A space-time swell track is defined by the successive position of an idealized wave packet travelling from the storm center at time $t = 0$ to a distance of 15000 km along the equator. At regular interval along this track, the wave spectrum is estimated by computing the spectral densities at a relative frequency resolution of 2% and a directional resolution of 0.5°. The quasi-analytic total wave energy is then obtained by summation over the spectrum, and compared to the asymptotic value.

The spatial decay of waves from such storms is thus completely specified by σ_x and γ_J. Due to the finite size of the storm source, the asymptotic decay should be attained in the limit $x \gg \sigma_x$. Further the dispersive decay requires a finite width of the wave spectrum but it is also affected by the size of the source. Indeed, the dispersive spreading induces travel distance differences of the order of $\delta_x = t\sigma_f \partial C_g/\partial f$. This corresponds to a difference in wave packet position δ_x at $t = 0$. The asymptotic decay is reached for $\delta_x \gg \sigma_x$. For a truly monochromatic source the energy decay is instead proportional to $1/\sin(\phi)$

In practice, beyond 4000 km from the source and for a large storm with $\sigma_x = 550$ km, the error relative the asymptotic decay is less than 0.4% for a Pierson-Moskowitz spectrum (defined by $\gamma_J = 1$), and 4.5% for a JONSWAP spectrum (defined by $\gamma_J = 3.3$). These two spectra correspond the the extremes of broad and narrow spectra in the open ocean, with the JONSWAP form being rather rare and corresponding more to a coastal or enclosed sea situation. For a very compact storm, with $\sigma_x = 220$ km the maximum error is 1.2% for a Pierson-Moskowitz spectrum and up to 9.6% (negative bias) for JONSWAP spectrum. Thus very compact storm with young waves may lead to a significant departure from the generic decay asymptote. however, such an extreme deviation is still several times smaller than the differences between observed decays and the conservative asymptotic decay. Further, error in source location gives an error proportional to the position mismatch divided by the distance from the source, and this effect is expected to be negligible.

These calculations were done for fixed storms. The reader is referred to (*2,3*), for a discussion of the effects of storm motion, that are likewise negligible.

2.3 Estimation of attenuation coefficients

In each ensemble of swell tracks, some SAR data was filtered out based on the following criteria

- the distance from the source should be more than 4000 km, in order to satisfy the point source hypothesis which gives a reference wave height decay to which observed decay is compared to estimate the attenuation, and also to minimize errors in the source localization.

- the wind speed should be more than 2 m s^{-1} and less than 10 m s^{-1}: this filters out weak wind conditions in which the waves are poorly imaged by the SAR, and high wind conditions in which the SAR modulation function may have larger errors.

- the measured wave height should be more than 0.6 m. This makes sure that the signal to noise ratio in the image is large enough so that the wave height estimation is accurate. Based on the validation of the SAR data, a lower threshold could have been chosen, but then one should also verify that the normalized variance of the image is within acceptable values (other features due to wind, rain, slicks may contaminate the wave spectrum estimate).

From this set of selected images, a function $H_s(\phi)$ was fitted. Two fits were performed, one with a constant linear decay α, the other with a constant non-linear decay γ. In each case the parameter α or γ was fitted together with the height $H_s(\phi_0)$ at a distance $x = R\phi_0 = 4000$ km from the storm source. In practice the possible values of $H_s(\phi_0)$, and α or γ were scanned and the pair (H_1, α) and (H_2, γ) that gave the minimum root mean square difference with $H_s(\phi)$ was retained (table 1). It should be noted that α and γ were found to be strictly positive in all cases.

In order to perform this fit, the function $H_s(\phi)$ was integrated numerically from $x = 4000$ to $x = 15000$ km, for each pair (H_1, α) or (H_2, γ), using a simple first order Euler scheme that was found to converge fast enough. The error function was computed by linearly interpolating the discretized $H_s(\phi_i)$ at the positions ϕ_j where selected observations were made.

3 Improvement in numerical wave modelling based on the present analysis

3.1 Model description

A very preliminary validation of a new wave model parameterization has been performed using the present results. Although relatively few tests have been carried out, one of the parameterizations turned out to outperform today's best wave models by a significant margin. This parameterization was thus implemented in the wave model routinely used at SHOM as part of the Previmer project, providing wave information to a variety of users (`http://www.previmer.org`). Further refinements will be performed. In particular this parameterization underestimates wave growth at relatively short fetches.

It should be noted that these result do not constitute a further proof of the correctness of the wave attenuation mechanism highlighted here, but rather gives an indication on the usefulness of this result, and of the order of magnitude of the effect on the entire sea state, and not just a few swell partitions. The model was therefore ran with three values of the dissipation factor f_e: 0, 0.0045 and 0.009.

Wave models are by no means perfect. They predict the wave spectrum based on the wave action balance equation (*4*), which writes in deep water,

$$\frac{dF(\mathbf{k})}{dt} = S_{\mathrm{in}}(\mathbf{k}) + S_{\mathrm{nl}}(\mathbf{k}) + S_{\mathrm{ds}}(\mathbf{k}). \tag{1}$$

Solving that equation presents a number of challenges. First of all, the wind-wave generation S_{in} and wave dissipation function S_{ds} are poorly known. Second, the better known non-linear interaction term $S_{\mathrm{nl}}(\mathbf{k})$ requires extensive computer power that make it impractical for routine wave forecasting. That term is thus usually parameterized with the approximate form $S_{\mathrm{nl}}^{\mathrm{DIA}}$ (*5*). Using that term may compensate for errors in the other two (*6, 7*) but the source terms are essentially uncertain in active wind wave generation, and their numerical integration is not simple either (*8*). Finally, the integration of the equation requires accurate numerical schemes when swells are to be propagated across ocean basins (*9*).

In previous work, it was found that the input term by Janssen (*10*) and used in the WAM-Cycle 4 model, probably has the right order of magnitude (*7, 11*). On top of this term, we now add a negative wind input term in order to represent the upward momentum flux associated with the wave attenuation observed here,

$$S_{\mathrm{in}}^{\mathrm{up}}(\mathbf{k}) = -\frac{\rho_a}{\rho_w} \max\left\{2k\sqrt{2\nu\sigma}, 16 f_e \sigma^2 u_{\mathrm{orb}}/g\right\} F(\mathbf{k}). \tag{2}$$

The first term is the linear viscous decay, and the second term is a parameterization for the nonlinear turbulent decay.

Thus the wind input source term reads

$$S_{in}\left(k,\theta\right) = \frac{\rho_a}{\rho_w}\frac{\beta_{\max}}{\kappa^2}\mathrm{e}^Z Z^4 \left(\frac{u_\star}{C}\right)^2 \cos^2(\theta-\theta_u)\sigma F\left(k,\theta\right) + S_{\mathrm{in}}^{\mathrm{up}}(\mathbf{k}), \tag{3}$$

where $\beta_{\max}$ is a non-dimensional growth parameter (constant), κ is von Kármán' constant. In the present implementation the air/water density ratio is constant. We define $Z = \log(\mu)$ where μ is given by Janssen (1991, eq. 16), and corrected for intermediate water depths, so that

$$Z = \log(kz_1) + \kappa / \left[\cos\left(\theta - \theta_u\right)\left(u_\star / C + z_\alpha\right)\right], \tag{4}$$

where z_1 is a roughness length modified by the wave-supported stress τ_w, and z_α is a wave age tuning parameter. z_1 is implicitly defined by

$$U_{10} = \frac{u_\star}{\kappa} \log\left(\frac{z_u}{z_1}\right) \tag{5}$$

$$z_0 = \max\left\{\alpha_0 \frac{\tau}{g}, 0.0015\right\} \tag{6}$$

$$z_1 = \frac{z_0}{\sqrt{1 - \tau_w/\tau}}. \tag{7}$$

The maximum value of z_0 was added to reduce the unrealistic stresses at high winds that are otherwise given by the standard parameterization. This is equivalent to setting a maximum wind drag coefficient of 2.5×10^{-3}.

As for the dissipation most previously proposed parameterization dissipate swells with the same formulation that is used for wave breaking, a parameterization which is clearly not supported by the present observations nor by the wave breaking statistics analyzed by others (*12*). We have thus chosen to use the simplest dissipation term formulated in terms of the direction-integrated spectral saturation $B\left(k\right)$

$$B\left(k\right) = \int_0^{2\pi} \sigma k^3 A(k, \theta) \mathrm{d}\theta, \tag{8}$$

with a realistic threshold $B_r = 1.2 \times 10^{-3}$ corresponding to the onset of wave breaking (*13*). That dissipation term takes the form

$$S_{\mathrm{ds}}(\mathbf{k}) = \sigma C_{\mathrm{ds}} \left[\max\left\{\frac{B\left(k\right)}{B_r} - B_r, 0\right\}\right]^2 F(\mathbf{k}). \tag{9}$$

We then adjusted the dissipation parameter $C_{\mathrm{ds}} = -2.2 \times 10^{-5}$. In order to obtain a reasonable balance of the source terms we also adjusted the wind-wave coupling coefficient

$\beta_{\max} = 1.25$, and the wave age correction factor $z_\alpha = 0.007$, instead of the values 1.2 and 0.011 typically used (*14*).

The model used to integrate the source term balance is the version 3.14 of WAVEWATCH III (*15*), with the modifications discussed here. The model was ran for the entire year 2006 with wind and sea ice concentration analyses from ECMWF (the sea ice data actually orginates from NOAA). The model grid resolution is 0.5 degree in latitude and longitude and the spectral discretization uses 24 directions and 32 frequencies exponentially spaced from 0.037 Hz to 0.07 Hz.

This model was run with three values of the swell friction factor f_e, namely 0.0, 0.045, 0.009. All other parameters were kept unchanged. The model was also ran with the parameterization used operationally at ECMWF and called here "BAJ" (*14*), in which the only change is that $\beta_{\max} = 1.25$ instead of $\beta_{\max} = 1.2$, to reduce a bias likely due to different numerical schemes and spatial resolutions in the ECWAM model used at ECMWF and the WAVEWATCH III model used here.

3.2 Model results and discussion

Here we illustrate the model performance with the bias against the altimeter-derived wave heights, normalized RMS errors at all buoys used in the JCOMM wave model comparison exercise (*16*). We further give more statistics in tables 2-4 for representative buoys, designated here by their World Meteorological Organization (WMO) identification number

- 62163 : Offshore of Westerrn France, North Atlantic. Large storms in winter and spring, some swells year round.
- 46001 : Offshore of Kodiak, AK. Large storms in winter, well exposed to all Pacific swells.

- 46005 : Offshore of Aberdeen, WA. Important storms in winter, well exposed to all Pacific swells.
- 41002 : South of Cape Hateras, 250 nautical miles East of Charleston, SC.
- 46069 : South of Santa Rosa Island, CA. Swell-dominated conditions.
- 51001 : North-west of Kauai, HI. Swell-dominated conditions.
- 51028 : Christmas Island, on the Equator, south of Hawaii. That buoys is exposed to most Pacific swells, and has local wind seas generated by trade winds. Local currents can be significant, and typically range from 0.3 to 1 m/s. These currents are not included in the present calculations, but can have a large effect on waves (*17*).

Based on these model calculations, it appears, that a likely range for the dissipation factor f_e applied to the total orbital velocity is 0.004–0.008. Such values are able to correct the wave height bias against the altimeter (figure S1) that exists with parameterizations that do not account for swell decay or the present parameterization with $f_e = 0$. In that latter case the maximum positive wave height biais in the Pacific reaches 1.2 m (not shown).

Figure S1 shows that the large bias in the East Pacific is partially corrected in the new model when using $f_e = 0.003$, although this is further improved when increasing f_e. Larger values of f_e, however tend to increase errors in other areas. The model likely underestimates the swell in their early stages and thus a more realistic attenuation eventually leads to an underestimation of the wave heights. The model with $f_e = 0.0045$ gives better results that using BAJ at most buoys (figure S2, table 2), at least in terms of correlations.

However, a constant and uniform value for f_e is probably not the best choice. Of particular interest is the last table with the low frequency wave heights....

Model run	BAJ	$f_e = 0$	$f_e = 0.0045$	$f_e = 0.009$
62163 NE	11.6	17.1	**10.5**	14.5
62163 NB	1.7	12.4	**-0.9**	-10.0
62163 r	0.9737	0.9684	0.9754	**0.9758**
46001 NE	**13.4**	24.3	14.1	19.4
46001 NB	**-2.1**	17.8	-5.1	-14.2
46001 r	0.9574	0.9414	**0.9584**	0.9570
46005 NE	12.4	33.3	**11.2**	15.9
46005 NB	3.1	30.2	**1.1**	-11.3
46005 r	0.9723	0.9634	**0.9743**	0.9739
41002 NE	**16.6**	22.1	17.9	24.4
41002 NB	**-9.1**	13.2	-11.1	-20.0
41002 r	0.9495	0.9343	**0.9499**	0.9483
46069 NE	**18.4**	33.9	18.6	31.5
46069 NB	**-11.5**	29.1	-12.2	-28.2
46069 r	0.9087	0.8738	0.9155	**0.9157**
51001 NE	**12.0**	34.0	**12.0**	24.6
51001 NB	**-5.0**	31.2	-5.8	-22.2
51001 r	0.9298	0.8894	**0.9331**	0.9314
51028 NE	12.5	49.4	**11.4**	31.5
51028 NB	-7.7	48.0	**-6.5**	-30.0
51028 r	0.8250	0.7488	**0.8370**	0.8266

Table 2: Model errors statistics on significant wave height for several model runs, at WMO buoys 62163, 65001, 41002, 51001, 65005, 46069 and 51028. NE stands for the r.m.s. error normalized by the r.m.s. observation, in %, NB stands for the bias normalized by the r.m.s. observation, in %, and r is Pearson's linear correlation coefficient. For each parameter the best model is highlighted in bold.

Model run	BAJ	$f_e = 0$	$f_e = 0.0045$	$f_e = 0.009$
62163 NE	9.9	11.3	**9.5**	13.2
62163 NB	**2.1**	-4.0	2.2	8.4
62163 r	0.8957	0.8762	0.9028	**0.9125**
46001 NE	9.2	20.5	**8.8**	10.2
46001 NB	-3.7	-16.2	-3.6	**2.8**
46001 r	0.8843	0.7416	**0.8893**	0.8816
46005 NE	12.8	26.1	13.0	**8.0**
46005 NB	-10.0	-22.5	-10.3	**-1.8**
46005 r	0.9007	0.7620	0.9034	0.9234
41002 NE	9.0	15.2	**8.4**	15.8
41002 NB	3.6	-11.5	**3.0**	11.0
41002 r	0.8554	0.7250	**0.8585**	0.8184
46069 NE	**11.4**	24.6	11.5	13.1
46069 NB	**-4.1**	-19.7	-5.0	7.1
46069 r	0.8565	0.7357	0.8610	**0.8842**
51001 NE	7.4	16.8	**7.1**	11.1
51001 NB	**-2.8**	-14.2	-3.2	6.0
51001 r	0.9128	0.8614	**0.9170**	0.9100
51028 NE	9.1	16.2	**8.6**	18.9
51028 NB	1.5	-13.0	**0.6**	15.4
51028 r	0.7316	0.5871	**0.7320**	0.7193

Table 3: Model errors statistics on mean frequency f_{02} for several model runs, at WMO buoys 62163, 65001, 41002, 51001, 65005, 46069 and 51028. Statistical parameters are defined in table 2.

Model run	BAJ	$f_e = 0$	$f_e = 0.0045$	$f_e = 0.009$
46001 NE	12.3	23.4	12.0	**10.4**
46001 NB	-7.2	-18.4	-6.7	**0.6**
46001 r	0.8377	0.6383	0.8402	**0.8553**
46005 NE	19.3	29.7	19.3	**11.3**
46005 NB	-15.3	-24.5	-15.1	**-6.8**
46005 r	0.8225	0.6151	0.8211	**0.8944**
41002 NE	8.3	18.4	**8.1**	14.2
41002 NB	0.4	-14.3	**0.2**	9.1
41002 r	**0.8630**	0.6816	0.8619	0.8408
46069 NE	13.8	23.6	13.7	**10.8**
46069 NB	-8.7	-18.2	-8.8	**2.2**
46069 r	0.8457	0.7410	0.8505	**0.8865**
51001 NE	9.8	16.8	**9.2**	9.3
51001 NB	-6.4	-13.5	-5.9	**2.1**
51001 r	0.8848	0.8147	0.8888	**0.8991**
51028 NE	8.6	13.3	**7.8**	11.2
51028 NB	-4.7	-10.7	**-4.1**	5.6
51028 r	0.8287	0.7412	0.8418	**0.8518**

Table 4: Model errors statistics on mean frequency f_{0-1} for several model runs, at WMO buoys 62163, 65001, 41002, 51001, 65005, 46069 and 51028. Statistical parameters are defined in table 2.

Model run	BAJ	$f_e = 0$	$f_e = 0.0045$	$f_e = 0.009$
46001 NE	**10.8**	12.0	**10.8**	12.1
46001 NB	**0.5**	0.9	-2.8	-4.9
46001 r	0.9247	0.9205	**0.9263**	0.9220
46005 NE	**9.8**	12.7	11.4	13.0
46005 NB	-3.8	**-2.4**	-6.8	-9.0
46005 r	0.9485	0.9388	**0.9493**	0.9448
41002 NE	13.4	14.3	**12.5**	13.2
41002 NB	3.3	4.5	**0.3**	-2.1
41002 r	0.9036	0.8979	**0.9052**	0.9036
46069 NE	**17.5**	16.8	18.1	20.1
46069 NB	-6.8	**-3.8**	-9.6	-12.1
46069 r	0.8699	0.8479	0.8704	**0.8729**
51001 NE	9.9	12.5	**9.7**	12.4
51001 NB	**-1.2**	2.5	-3.9	-6.6
51001 r	0.9399	0.9130	**0.9411**	0.9365
51028 NE	21.4	25.5	**20.3**	19.5
51028 NB	11.3	15.3	8.8	**6.5**
51028 r	0.7932	**0.8039**	0.7932	0.7842

Table 5: Model errors statistics on high frequency wave height (0.3–0.49 Hz). Buoy locations and statistical parameters are defined in table 2.

Model run	BAJ	$f_e = 0$	$f_e = 0.0045$	$f_e = 0.009$
46001 NE	35.0	63.5	**33.4**	34.2
46001 NB	11.8	52.0	**6.8**	-10.3
46001 r	**0.8972**	0.8670	0.8946	0.8960
46005 NE	39.3	78.1	35.1	**24.7**
46005 NB	28.7	73.6	25.3	**3.3**
46005 r	0.9431	0.9389	**0.9478**	0.9465
41002 NE	**43.4**	55.8	48.4	52.8
41002 NB	**-4.6**	20.7	-11.1	-22.4
41002 r	**0.8548**	0.7841	0.8275	0.8348
46069 NE	24.5	65.5	**24.1**	35.7
46069 NB	2.2	59.1	**1.2**	-25.4
46069 r	0.9009	0.8610	0.9073	**0.9163**
51001 NE	27.4	61.6	**25.3**	29.1
51001 NB	11.2	55.6	**7.7**	-16.6
51001 r	0.9007	0.8925	0.9044	**0.9073**
51028 NE	23.7	77.8	**22.2**	32.9
51028 NB	7.3	72.7	**5.8**	-26.7
51028 r	0.7853	0.7703	0.8036	**0.8135**

Table 6: Model errors statistics on low frequency wave height (0.037–0.08 Hz). Buoy locations and statistical parameters are defined in table 2.

References

1. P. Wessel, W. H. F. Smith, *J. Geophys. Res.* **101**, 8741 (1996).
2. W. H. Munk, G. R. Miller, F. E. Snodgrass, N. F. Barber, *Phil. Trans. Roy. Soc. London A* **255**, 505 (1963).
3. F. E. Snodgrass, *et al.*, *Phil. Trans. Roy. Soc. London* **A249**, 431 (1966).
4. G. J. Komen, *et al.*, *Dynamics and modelling of ocean waves* (Cambridge University Press, Cambridge, 1994).
5. S. Hasselmann, K. Hasselmann, J. Allender, T. Barnett, *J. Phys. Oceanogr.* **15**, 1378 (1985).
6. M. L. Banner, I. R. Young, *J. Phys. Oceanogr.* **24**, 1550 (1994).
7. F. Ardhuin, *et al.*, *J. Phys. Oceanogr.* **37**, 908 (2007).
8. J. C. Hargreaves, J. D. Annan, *J. Atmos. Ocean Technol.* **18**, 711 (2000).
9. H. L. Tolman, *Ocean Modelling* **4**, 269 (2002).
10. P. A. E. M. Janssen, *J. Phys. Oceanogr.* **21**, 1631 (1991). See comments by D. Chalikov, J. Phys. Oceanogr. 1993, vol. 23 pp. 1597-1600.
11. M. L. Banner, R. P. Morison, *Proceedings of the 9th International workshop on wave hindcasting and forecasting, Victoria, Canada* (2006).
12. M. L. Banner, A. V. Babanin, I. R. Young, *J. Phys. Oceanogr.* **30**, 3145 (2000).
13. A. V. Babanin, I. R. Young, *Proceedings of the 5th International Symposium Ocean Wave Measurement and Analysis, Madrid, june 2005* (ASCE, 2005). Paper number 51.

14. J. Bidlot, S. Abdalla, P. Janssen, A revised formulation for ocean wave dissipation in CY25R1, *Tech. Rep. Memorandum R60.9/JB/0516*, Research Department, ECMWF, Reading, U. K. (2005).

15. H. L. Tolman, *Proceedings, 10th Int. Workshop of Wave Hindcasting and Forecasting, Hawaii* (2007).

16. J.-R. Bidlot, *et al.*, *Proceedings, 10th Int. WOrkshop of Wave Hindcasting and Forecasting, Hawaii* (2007).

17. N. Rascle, F. Ardhuin, P. Queffeulou, D. Croizé-Fillon, *Ocean Modelling* (2008). Submitted. Available at http://hal.archives-ouvertes.fr/hal-00201380/.

18. SAR data was kindly provided by the European Space Agence which also funded their analysis.

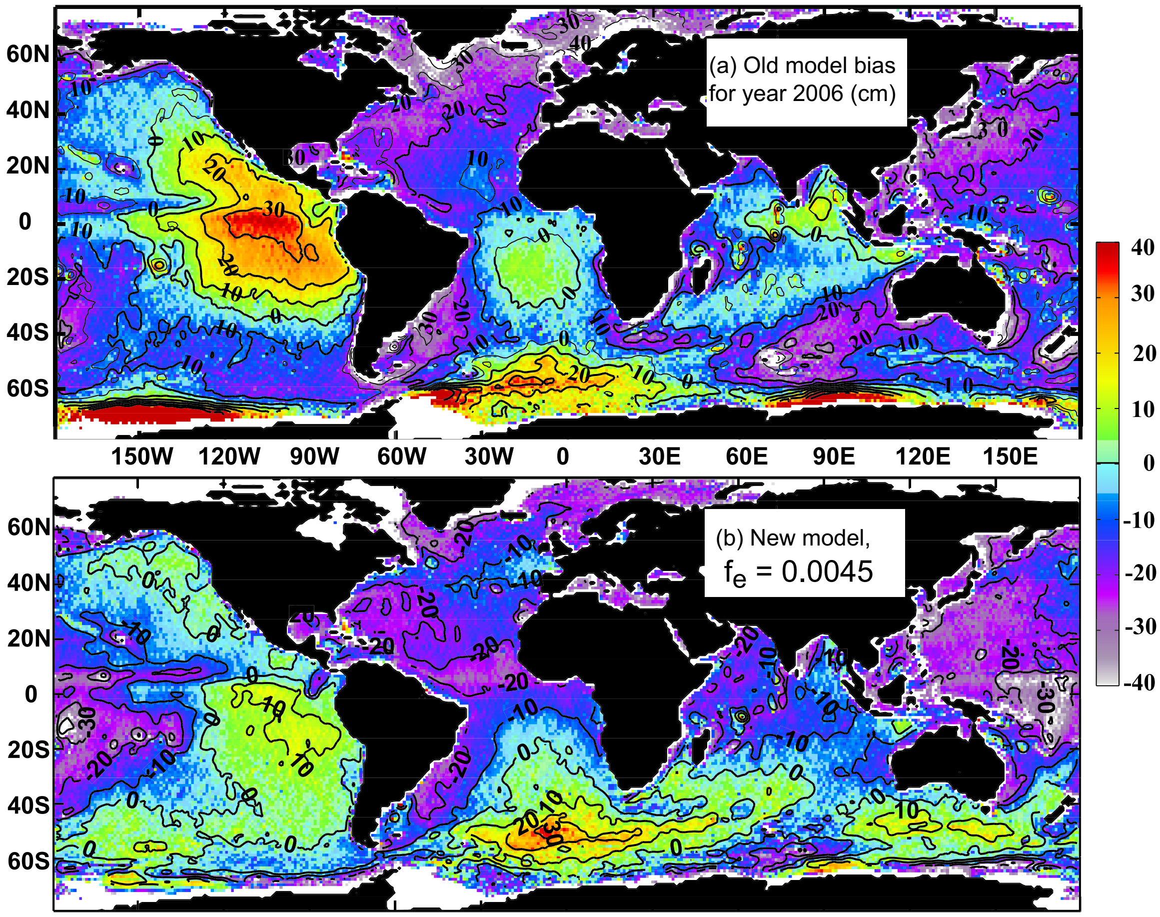

Figure 1: (a) Model bias using the BAJ parameterization for 2004 to 2006, combining data from JASON, ENVISAT and GEOSAT-Follow On (GFO), see Rascle et al. 2008, Appendix B for satellite data analysis methods. (b) difference between the new model with $f_e = 0.003$ and the BAJ run for the year 2006, added to the difference shown in (a).

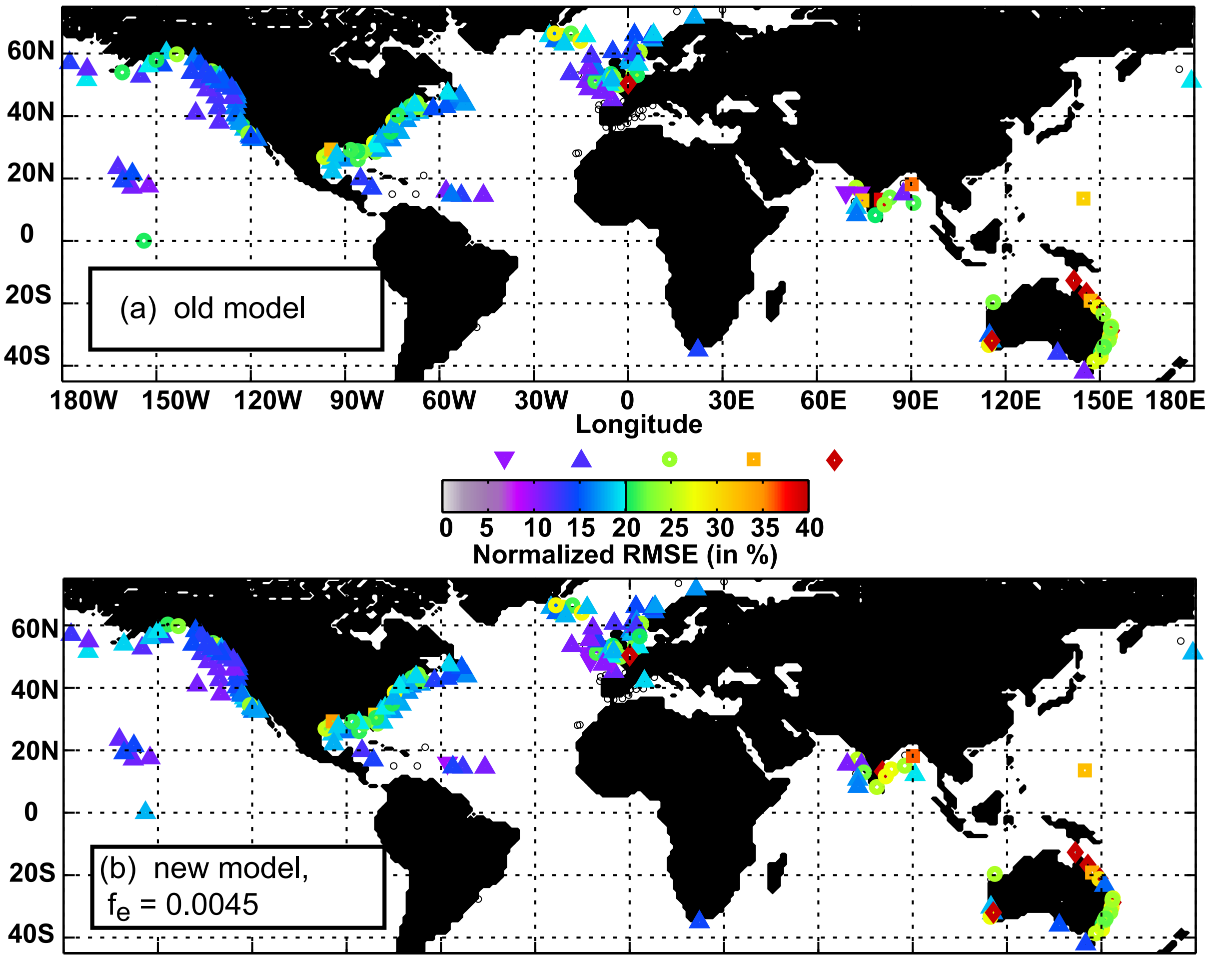

Figure 2: Statistics for the year 2006. Using the same model with WAM-Cycle 4 type parameterization (*14*) gives (a) normalized RMSE for H_s at in situ locations. Symbols ∇, $\triangle$, $\circ$, , and $\diamondsuit$ correspond to values in the ranges $0 \leq x < 10$, $10 \leq x < 20$, $20 \leq x < 30$, $30 \leq x < 40$, $40 \leq x$. (b) Same as (a) but with the parameterization proposed here, using $f_e = 0.003$.